Range Prediction and Extension for Automated Electric Vehicles with Fail-Operational Powertrain

Optimal and Safety Based Torque Distribution for Multiple Traction Motors

Kirill Gorelik, Ahmet Kilic
Corporate Sector Research and Advance Engineering
Robert Bosch GmbH
Renningen, 71272, Germany
Email: {kirill.gorelik, ahmet.kilic}@de.bosch.com

Roman Obermaisser
Institute of Embedded Systems
University of Siegen
Siegen, 57068, Germany
Email: roman.obermaisser@uni-siegen.de

***Abstract*—With the introduction of robocabs and automated shuttles new requirements for vehicle powertrain arise requiring fail-operational system behavior. Redundancy in powertrain components can be used for the increase of driving efficiency, but requires also new strategies for controlling powertrain topologies with independent traction batteries. This paper presents a new concept and algorithm for the optimal torque distribution based on multi-objective optimization problem. The first objective of the optimization problem is to increase the driving energy efficiency by torque distribution between front and rear axle as well as between left and right side motors. A symmetrical discharge of the independent batteries is considered as a second objective. Using the runtime powertrain diagnostics, the torque distribution strategy covers also possible failure case operation. An optimal torque distribution profile as well as required propulsion energy are predicted for the entire driving cycle online. This information is then used for safety based range extension allowing to arrive at the safest possible location for the passengers also in case of a failure. Simulation results for different normal and failure case scenarios show a significant increase of driving efficiency while ensuring symmetrical discharge of the independent traction batteries.**

Keywords—Automated Driving, Electric Vehicles, Energy Management System, Fail-Operational, Functional Safety, Optimal Torque Distribution, Range Extension, Range Prediction.

I. INTRODUCTION

Robocabs and automated shuttles will play a big role in the future mobility. According to the study by Roland Berger approximately one third of the worldwide kilometers will be driven by robocabs in 2030 [1]. The introduction of highly and fully (SAE level 4 and 5) automated driving requires fail-operational system behavior, since the driver must not be able to take over the vehicle control in case of a failure according to the automation levels introduced by SAE [2]. Therefore, new safety requirements arise for the subsystems responsible for the execution of the automated fallback driving task. The functional safety norm ISO 26262:2011 requires the design of such systems with corresponding automotive safety integrity level (ASIL) [3]. New fail-operational power net topologies fulfilling the high safety requirements were developed [4], requiring also new concepts and strategies for their control.

An energy management system with automated fault reactions controlling fail-operational power nets was proposed in [5, 6]. The introduction of robocabs and automated shuttles requires also new fail-operational powertrain topologies enabling vehicle operation also in case of a system failure. The powertrain topology and control should enable the arrival of the passengers at a safe state location. The concept of safety based range extension with the goal of arriving at the safest possible location for the passengers was presented in [5, 7]. Fail-operability of a powertrain requires redundancies of the components and brings also new degrees of freedom for the control of such topologies.

A lot of work was investigated in the control strategies of multiple traction motors topologies. The authors of [8] propose an online torque distribution strategy for disengaging one motor in low torque regions for a front and rear axle propelled powertrain topology. A control strategy for energy efficient torque distribution was also proposed in [9, 10]. An offline optimization is used for estimating the optimal torque distribution factor between front and rear axle and generating a look-up table, which is then used for online optimal control increasing the energy efficiency and comfort [10]. In [11], an adaptive particle swarm optimization algorithm is used for solving the multi-objective torque distribution problem for four in-wheel motors powertrain topology considering the energy efficiency and vehicle dynamics. The authors of [12] propose a real-time torque distribution strategy using also particle swarm optimization for a powertrain topology with a front axle traction motor and two rear in-wheel motors with the main goal of driving efficiency increase.

The proposed torque distribution strategies have in common that they are not considering the failure case operation. The traction motors are also supplied by one traction battery only. The work presented in this paper considers fail-operational powertrain topologies with two independent traction batteries for front and rear axle and two motors per axle. The torque distribution algorithm proposed in this work considers the normal and failure case operation and predicts torque distribution profile for the entire route to the safe stop location online. The predicted torque distribution profile and the corresponding predicted propulsion energy is then used by

978-1-5386-3664-0/18/$31.00 ©2018 IEEE

the energy management system for the optimization of the energy flow in the powertrain for safety based range extension.

In Section II of this paper, a brief overview over the architecture and functionality of the energy management system as presented in [5, 6] is given. Based on the electronic horizon, a driving trajectory to the safe stop location is predicted. The concept of dynamic driving trajectory prediction as presented in [7] will be briefly summarized.

For a given driving trajectory, an optimal torque distribution profile for fail-operational powertrain topology with two motors per axle and two independent batteries is predicted by solving the multi-objective optimization problem, increasing so the driving energy efficiency and the symmetry of the discharge of the independent traction batteries. A mathematical model of fail-operational powertrain as well as the definition of the optimization problem are presented in Section III. Simulation results for normal and failure case operation and control of the powertrain using the proposed torque distribution algorithm conclude this work.

II. Energy Management System

An optimal and adaptive energy management system (EMS) for the real-time control of fail-operational power nets with automated fault reactions was presented in [5]. The main goal of this EMS is the safety based range extension, meaning that the power net energy flow is optimized in a way allowing to arrive at the safest possible location, which could for example be the driving destination set by the passenger, parking area, emergency stop bay etc. [5]. Based on a predicted driving cycle, the required propulsion energy (E_{pr}) to the destination is estimated as well as the energy needed by the safety (E_{rs}) and comfort loads (E_{rc}). After predicting the remaining energy resources (E_{bat}) of the power net, the overall energy flow is optimized. The architecture of the energy management system is illustrated in Fig. 1.

A. Driving Trajectory Prediction

Using dynamic map data [13] and current vehicle position, an electronic horizon extending the vehicle view by the knowledge about the route coming ahead [14, 15] can be provided to map based applications using the ADASISv2 protocol [14, 15]. The transmission of static map data should be extended to dynamic map data in the new version of the protocol (ADASIS v3) [13]. Depending on the application, the ADAS horizon provider can transmit different electronic horizon profiles. For the dynamic route prediction the use of the profiles containing velocity limits, road slope, stops and the safe stop locations is proposed [7]. Based on the current vehicle position and velocity, a driving trajectory to the safe stop location is predicted as presented in [7]. The output of the driving trajectory prediction contains an array of the structure as illustrated in Fig. 2. Each segment i of the predicted driving trajectory contains a constant acceleration value (a[i]), a constant road slope value (sl[i]) and the duration of this segment ($dT_{seg}[i]$). Using this information, the velocity profile can be constructed for the prediction of propulsion energy and torque distribution.

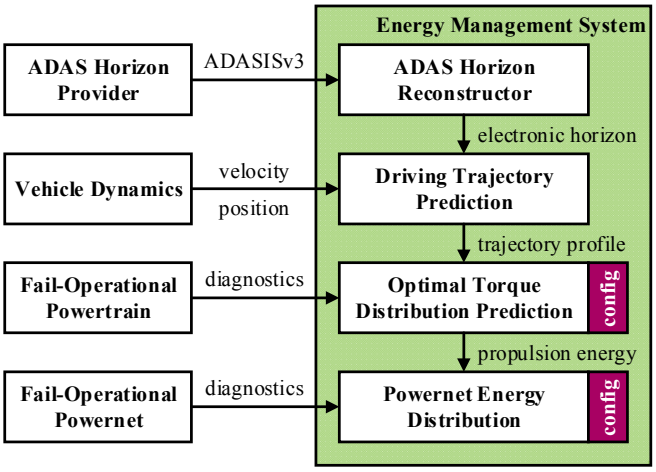

Fig. 1. Architecture of torque distribution prediction algorithm.

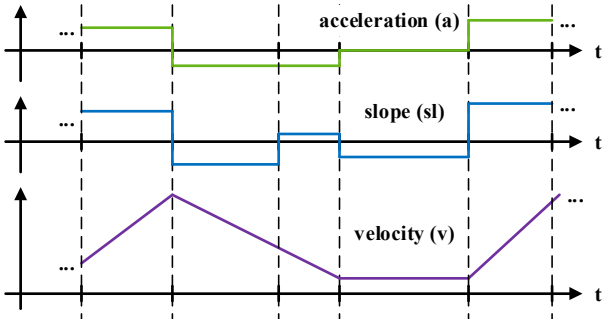

index	...	i-2	i-1	i	i+1	i+2	...	[-]
dT[i]	...	1.20	1.40	0.80	1.70	1.10	...	[s]
a[i]	...	0.75	-0.50	-0.50	0.0	1.00	...	[m/s^2]
sl[i]	...	2.0	-1.5	0.5	-1	-2.5	...	[%]

Fig. 2. Structure of predicted driving trajectory.

B. Optimal Torque Distribution Prediction

For powertrain topologies with multiple motors the required propulsion energy for completing a given driving cycle depends on the torque distribution strategy. Furthermore, runtime changes in the components due to possible failures (e.g. decrease of motor efficiency or battery power) influence also the required propulsion energy. Therefore, an accurate propulsion energy prediction requires also online torque distribution prediction for the entire driving trajectory, considering also the current powertrain state. The predicted propulsion energy is then used as input for the energy flow optimization. The concept for the optimal torque distribution profile is presented in detail in Section III.

C. Energy Flow Optimization

For the energy flow optimization it is assumed that the entire power net consists of up to n ($n \geq 1$) sub power nets (spn), which could have energy resources, propulsion, safety and comfort components. Denoting the energy flow from sub power net i to k ($i \neq k$) by $E_{out,ik}$ with the efficiency η_{ik} and from k to i by $E_{out,ki}$, the energy balance equation can be set up for each sub power net k [5, 6]:

$$E_{spn,k}(\cdot) = \sum_{\substack{i=1,i\neq k \\ i\in OPR}}^{n} (\eta_{ik} E_{out,ik} - E_{out,ki}) + (E_{bat,k} - E_{rs,k} - E_{rc,k} - E_{pr,k}) \quad (1)$$

The set of all operational sub power nets is denoted by OPR (**OP**e**R**ational), the set of all sub power nets with available energy resources exceeding the internal energy demands by SRC (**S**ou**RC**e). Using this notation, the energy flow optimization problem can be defined as [5, 6]:

$$\max_{(\cdot)} \sum_{i=1,i\in SRC}^{n} E_{spn,i}(\cdot) \quad \text{s.t.} \begin{cases} 0 \le E_{spn,i}(\cdot), & i \in \{1..n\} \\ 0 \le E_{out,ik}, & i,k \in \{1..n\}, i \neq k \end{cases} \quad (2)$$

The first inequality constraint of the optimization problem forces the solver to find a solution for power net energy distribution in a way that the energy demands are covered by the available energy resources. The second constraint results from the definition of the energy flow direction.

If no solution for the energy flow optimization problem is found, a three level degradation concept for reducing the overall system energy demand is proposed in [5] corresponding to the definition of the safety based range extension. On the first level the comfort loads are degraded. If still no solution exists, the maximum allowed velocity and acceleration are degraded resulting in the decrease of propulsion energy. Only on the last level of the degradation concept the driving destination (safe stop location) is degraded.

III. Multiple Motors Torque Distribution Prediction

The concept and algorithm used for the prediction of the optimal safety based torque distribution for multiple motors is presented in this section. A brief overview of a fail-operational powertrain topology used for the analysis in this work is given in Part A of this section. The model of the fail-operational powertrain required for the definition of the torque distribution optimization problem is presented in Part B. The definition of the optimization problem as well as the algorithm used for the prediction of the torque distribution profile for the entire driving cycle are presented in Part C and D.

A. Fail-Operational Powertrain Topology

For the analysis in this work, the fail-operational powertrain topology is assumed to be as illustrated in Fig. 3. It consists basically of two independent axles which are controlled separately. Each axle has its own power supply (traction battery), one gear box and two electrical machines ($EM_{\{xy\}}$) which can be disengaged by the corresponding clutches ($CL_{\{xy\}}$). The axles should be dimensioned in a way that in case of a sudden failure of one axle the vehicle can be brought to a safe state with the remaining functional axle. Since the both traction batteries are not interconnected, it should be ensured by the control strategy that the batteries are not discharged asymmetrically.

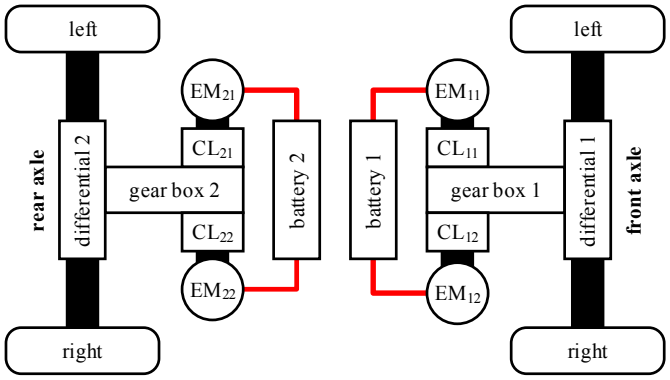

Fig. 3. Fail-operational powertrain topology.

B. Fail-Operational Powertrain Model

The prediction of the optimal torque distribution used for the estimation of required propulsion energy for completing a driving cycle and safety based range extension is based on a simple powertrain model considering the longitudinal vehicle dynamics. The powertrain model consists of a gear box with constant gear ratio, electrical machine and traction battery model. As shown in Section II.A, the predicted driving trajectory is divided into segments with constant acceleration value (a) and road slope (sl). Assuming a constant vehicle acceleration a_i for the duration of dT_i and the vehicle velocity v_i at the time instant t_i, the average required vehicle traction force $F_{t,i}$ can be approximated as [7, 16]:

$$F_{t,i} \approx m a_i + \frac{\rho A_f c_d}{2}\left(v_i + \frac{a_i dT_i}{2}\right)^2 + mg\frac{c_r + sl_i}{\sqrt{sl_i^2 + 1}} \quad (3)$$

The vehicle mass is denoted by m, vehicle frontal area by A_f, rolling friction and aerodynamic drag coefficients by c_r and c_d, gravitational force by g and ambient air density by ρ. The average required wheel torque $T_{w,i}$ and wheel speed $\omega_{w,i}$ at the time instant t_i with wheel radius r_w can be calculated as [7, 16]:

$$\omega_{w,i} = r_w^{-1}\left(v_i + \frac{a_i dT_i}{2}\right), \quad T_{w,i} = r_w F_{t,i} \quad (4)$$

As proposed in [9, 10], the total required wheel torque $T_{w,i}$ can be distributed between the front and rear axle using the distribution factor $\alpha_{fr,i}$. The front wheel ($T_{wf,i}$) and rear wheel ($T_{wr,i}$) torque is then defined as:

$$T_{wf,i} = \alpha_{fr,i} T_{w,i}, \quad T_{wr,i} = (1 - \alpha_{fr,i}) T_{w,i} \quad (\alpha_{fr,i} \in [0..1]) \quad (5)$$

Having two electrical machines at each axle, the fail-operational powertrain topology as depicted in Fig. 3 provides additional degrees of freedom for torque distribution strategy. The required front ($T_{wf,i}$) and rear wheel ($T_{wr,i}$) torque can be distributed between left and right side electrical machines using the distribution factor $\alpha_{\{x\}lr,i}$ with index x = f for front and x = r

for rear axle. The required left ($T_{em\{x\}l,i}$) and right side ($T_{em\{x\}r,i}$) electrical machine torque can be then defined as:

$$\begin{aligned} T_{em\{x\}l,i} &= k_{gb\{x\},i}\alpha_{\{x\}lr,i}T_{w\{x\},i} \\ T_{em\{x\}r,i} &= k_{gb\{x\},i}(1-\alpha_{\{x\}lr,i})T_{w\{x\},i} \end{aligned} \quad (\alpha_{\{x\}lr,i} \in [0..1]) \qquad (6)$$

By assuming fixed gear ratio ($\gamma_{gb\{x\}}$) and efficiency ($\eta_{gb\{x\}}$), the gear box transmission factor $k_{gb\{x\},i}$ for front (x = f) and rear (x = r) axle gear box can be defined as:

$$k_{gb\{x\},i} = \begin{cases} \gamma_{gb\{x\}}^{-1}\, c_{gb\{x\},i}^{-1}\eta_{gb\{x\}}^{-1}, & T_{w\{x\},i} \geq 0 \\ \gamma_{gb\{x\}}^{-1} c_{gb\{x\},i}\,\eta_{gb\{x\}}, & T_{w\{x\},i} < 0 \end{cases} \qquad (7)$$

The factor $c_{gb\{x\},i} \in [0,1]$ is used for modeling gear box failures resulting in decrease of transmission efficiency. Using the definitions above, the left (y = l) and right (y = r) side electrical machine angular speed can be defined as:

$$\omega_{em\{xy\},i} = \begin{cases} 0, & CL_{\{xy\},i} = 0 \\ \gamma_{gb\{x\}}\omega_{w,i}, & CL_{\{xy\},i} = 1 \end{cases} \qquad (8)$$

The factor $CL_{\{xy\},i}$ defines the state of the corresponding electrical machine clutch. If the clutch is engaged, the factor $CL_{\{xy\},i}$ is set to 1, otherwise to 0. Using (6) and (8), the required electrical power for each electrical machine in motor ($T_{em\{xy\},i} > 0$) and generator mode ($T_{em\{xy\},i} < 0$) can be calculated with:

$$P_{em\{xy\},i} = \begin{cases} c_{em\{xy\},i}^{-1}\eta_{em\{xy\},i}^{-1}\omega_{em\{xy\},i}T_{em\{xy\},i}, & T_{em\{xy\},i} > 0 \\ c_{em\{xy\},i}\eta_{em\{xy\},i}\omega_{em\{xy\},i}T_{em\{xy\},i}, & T_{em\{xy\},i} < 0 \end{cases} \qquad (9)$$

The electrical machine efficiency $\eta_{em\{xy\},i}$ is a function of rotational speed, required torque and electrical machine supply voltage. It is estimated using look-up functions for efficiency map and can be scaled with the factor $c_{em\{xy\},i} \in [0,1]$ modeling so the possible electrical machine failures resulting in efficiency decrease. The required battery power $P_{bat\{x\},i}$ for front (x = f) and rear axle battery (x = r) can be then defined as:

$$P_{bat\{x\},i} = P_{em\{x\}l,i} + P_{em\{x\}r,i} \qquad (10)$$

Using an equivalent circuit model for the battery consisting of open circuit voltage source $V_{oc\{x\},i}$ and battery internal resistance $R_{in\{x\},i}$ [16], the battery terminal voltage $V_{bat\{x\},i}$ can be calculated as:

$$V_{bat\{x\},i} = V_{oc\{x\},i} - c_{rin\{x\},i}R_{in\{x\},i}I_{bat\{x\},i} \qquad (11)$$

The factor $c_{rin\{x\},i} \geq 1$ is used for modeling battery failures resulting in increase of battery internal resistance (decrease of battery terminal power). The battery terminal current can be calculated as:

$$I_{bat\{x\},i} = \frac{V_{oc\{x\},i} - \sqrt{V_{oc\{x\},i}^2 - 4\,P_{bat\{x\},i}c_{rin\{x\},i}R_{in\{x\},i}}}{2\,c_{rin\{x\},i}R_{in\{x\},i}} \qquad (12)$$

The battery state of charge $SoC_{\{x\},i+1}$ at the time instant t_i+dT_i can be then estimated as:

$$SoC_{\{x\},i+1} = SoC_{\{x\},i} - \frac{I_{bat\{x\},i}dT_i}{c_{qbat0\{x\},i}Q_{bat0\{x\}}} \qquad (13)$$

The factor $c_{qbat0\{x\},i} \in [0,1]$ is used for modeling battery failures resulting in decrease of battery nominal capacitance Q_{bat0}. The presented powertrain model is used for the definition of torque distribution optimization problem as presented in the next part of this section.

C. Definition of Torque Distribution Optimization Problem

As shown in Section II, one of the main goals of the energy management system is to optimize the energy flow in the vehicle power net in a way allowing to arrive at the safest possible position. Since the fail-operational powertrain topology as illustrated in Fig. 3 has two independent batteries, the energy efficient wheel torque distribution between front and rear axle could lead to the case that the batteries are discharged asymmetrically. Assuming the worst case of fully asymmetrical discharge of front and rear battery, a spontaneous failure of the full battery would lead to the violation of the defined energy management goal of arriving at safest possible position. Therefore, by optimizing the torque distribution for the safety based range extension, it should be ensured that the state of charge of front and rear battery is almost the same during the entire driving cycle. By optimizing the energy flow under consideration of nearly symmetrical batteries discharge, nearly the same vehicle range for driving in degraded mode in case of a failure of one axle can be guaranteed. By considering the difference in state of charge of front and rear battery, the torque distribution optimization problem for each time interval $[t_i, t_i+dT_i)$ can be defined as:

$$\begin{aligned} \max_{(\cdot)} \quad & SoC_{f,i+1}(\alpha_{fr,i},\alpha_{flr,i}) + SoC_{r,i+1}(\alpha_{fr,i},\alpha_{rlr,i}) - \\ & \beta_{dSoC}\left|SoC_{f,i+1}(\alpha_{fr,i},\alpha_{flr,i}) - SoC_{r,i+1}(\alpha_{fr,i},\alpha_{rlr,i})\right| \\ \text{s.t.} \quad & \begin{cases} SoC_{\{x\},min} \leq SoC_{\{x\},i+1} \leq SoC_{\{x\},max} \\ I_{bat\{x\},chrg,max} \leq I_{bat\{x\},i} \leq I_{bat\{x\},dcha,max} \\ V_{bat\{x\},min} \leq V_{bat\{x\},i} \leq V_{bat\{x\},max} \\ T_{em\{xy\},gen,max,i} \leq T_{em\{xy\},i} \leq T_{em\{xy\},mot,max,i} \\ P_{em\{xy\},gen,max,i} \leq P_{em\{xy\},i} \leq P_{em\{xy\},mot,max,i} \end{cases} \end{aligned} \qquad (14)$$

By maximizing the sum of the state of charges of front and rear battery as a function of torque distribution factors $\alpha_{fr,i}$ (front/rear torque distribution) and $\alpha_{flr,i}/\alpha_{rlr,i}$ (left/right torque distribution for front and rear axle), the driving energy efficiency can be increased. By subtracting the absolute value of the delta state of charge scaled with the factor β_{dSoC} from the first objective, the solver can be forced to keep the difference between front and rear battery state of charge low. For high values of scaling factor β_{dSoC}, the torque distribution can be

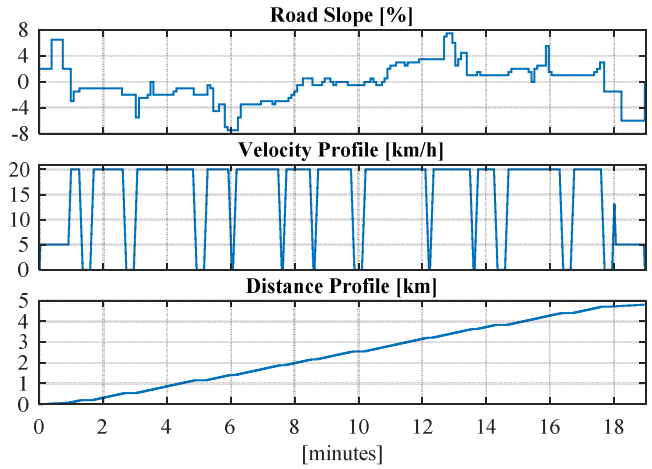

Fig. 4. Driving cycle for simulation results.

optimized for symmetrical batteries discharge. For low values of β_{dSoC}, a small asymmetry in batteries discharge can be tolerated for the sake of higher driving energy efficiency as will be shown with simulation results in Section IV.

To ensure the operation of traction batteries and electrical machines within the specified conditions, the objective function must be maximized under inequality constraints as defined in (14). By charging and discharging the traction batteries, the battery state of charges should remain within the specified minimum ($SoC_{\{x\},min}$) and maximum ($SoC_{\{x\},max}$) bounds. According to the definition in (12), the battery output current is positive in case of discharge and negative in case of battery charge. By maximizing the objective function, the battery output current should be less than maximum allowed discharge current $I_{bat\{x\},dcha,max}$ and greater than maximum allowed charge current $I_{bat\{x\},chrg,max}$. For avoiding the under- and overvoltage in the power net, also the battery output voltage should be within the specified range between minimum ($V_{bat\{x\},min}$) and maximum ($V_{bat\{x\},max}$) allowed battery output voltage. Also the output torque and power of each electrical machine should be bounded to the range defined by the maximum allowed torque/power in generator ($T_{em\{xy\},gen,max,i}$ / $P_{em\{xy\},gen,max,i}$) and motor ($T_{em\{xy\},mot,max,i}$ / $P_{em\{xy\},mot,max,i}$) mode.

By solving the optimization problem as defined in (14) for each interval of the driving trajectory, the predicted torque distribution profile for the entire driving cycle can be calculated as presented in the next part of this section.

D. Torque Distribution Prediction Algorithm

As shown in Section II.A, the predicted driving trajectory is divided into segments with constant acceleration and slope values. For each of these segments the optimization problem as defined in (14) can be solved. At the beginning of the torque distribution prediction, the measured battery state of charge, battery output current and supply voltage of the electrical machines are taken as input parameters for solving the optimization problem for the first entry of the predicted driving trajectory. The solution of the optimization problem defines a fixed torque distribution between front and rear axle as well as between left and right side electrical machines for each axle for the time interval $[t_i, t_i+dT_{seg,i})$. Using these torque distribution factors, the initial battery state of charge, battery output current as well as the supply voltage for the next segment of the driving trajectory can be predicted. These values are then used as input for solving the optimization problem as defined in (14) for the second segment of the driving trajectory. This process is repeated for each segment of the driving trajectory.

As proposed in [7], a variable calculation time step $dT_{calc,i}$ can be used for reducing the computational effort. For the segments with the segment acceleration $a_{seg,i} = 0$, the calculation step is set to the current segment duration $dT_{seg,i}$. For the segments of the driving trajectory with $a_{seg,i} \neq 0$, the prediction of the torque distribution is divided into j steps depending on the minimum specified calculation step dT_{min} [7]:

$$dT_{calc,i} = \begin{cases} dT_{seg,i}, & a_{seg,i} = 0 \\ \dfrac{dT_{seg,i}}{j}, & a_{seg,i} \neq 0,\ j = ceil\left(\dfrac{dT_{seg,i}}{dT_{min}}\right) \end{cases} \quad (15)$$

For solving the optimization problem as defined in (14), the torque distribution factors can be considered as continuous or as discrete valued. In case of discrete values, the set A_x, containing linearly spaced discrete values can be defined as:

$$A_x = \left\{ \alpha_x \mid \alpha_x \in [0,1] \wedge \alpha_x = \frac{n}{|A_x|-1} \wedge n \in \aleph_0 \right\} \quad (16)$$

The number of elements in the set A_x is denoted by $|A_x|$ (cardinality of the set A_x, $A_x > 1$). In the next section, simulation results for various cardinalities of front/rear (A_{fr}) and left/right (A_{lr}) torque distribution sets as well as for different operating conditions will be presented and discussed.

IV. Simulation Results

The simulation results for three different scenarios are presented in this section. For the simulation results in scenario 1 it is assumed that the initial battery state of charge for front and rear axle are symmetrical. Scenario 2 exemplifies the behavior of the torque distribution control for the case of asymmetrical initial battery state of charges. Simulation results in scenario 3 exemplify the behavior of the proposed torque distribution strategy for a failure case assuming the efficiency decrease in front left electrical machine of the powertrain topology as illustrated in Fig. 3.

For each scenario, a driving cycle as shown in Fig. 4 is assumed, which is based on a real logged route. For each scenario, the simulations are executed by varying the cardinality value for the factor set for front/rear (A_{fr}) and for left/right (A_{lr}) torque distribution. For the cardinality value $|A_x| = 1$, the torque is assumed to be equally distributed ($\alpha_x \in \{0.5\}$). For the cardinality value $|A_x| = 3$ three discrete values ($\alpha_x \in \{0, 0.5, 1\}$) and for $|A_x| = 11$ eleven discrete values ($\alpha_x \in \{0, 0.1, \ldots, 1\}$) for torque distribution factor are considered. The simulation results are summarized in tables containing the battery state of charge for front and rear axle at the end of the driving cycle (SoC_{end}), average delta state of charge

considering both axles as well as the deviation of the average delta state of charge relative to the value for equal torque distribution between front and rear axle ($|A_{fr}| = 1$) and between left and right side electrical machines ($|A_{lr}| = 1$).

TABLE I. SYMMETRICAL INITIAL BATTERY SOCS ($B_{DSoC} = 0.0$)

β_{dSoC} = 0.0	Front Battery SoC_{end} [%]			Rear Battery SoC_{end} [%]		
	$\|A_{lr}\| = 1$	$\|A_{lr}\| = 3$	$\|A_{lr}\| = 11$	$\|A_{lr}\| = 1$	$\|A_{lr}\| = 3$	$\|A_{lr}\| = 11$
$\|A_{fr}\| = 1$	75.822	76.255	76.255	75.822	76.255	76.255
$\|A_{fr}\| = 3$	76.192	76.232	76.232	76.192	76.521	76.521
$\|A_{fr}\| = 11$	76.197	76.232	76.232	76.187	76.525	76.525
β_{dSoC} = 0.0	Average Battery dSoC [%]			dSoC Deviation [%]		
	$\|A_{lr}\| = 1$	$\|A_{lr}\| = 3$	$\|A_{lr}\| = 11$	$\|A_{lr}\| = 1$	$\|A_{lr}\| = 3$	$\|A_{lr}\| = 11$
$\|A_{fr}\| = 1$	4.178	3.745	3.745	0	-10.376	-10.376
$\|A_{fr}\| = 3$	3.808	3.624	3.624	-8.854	-13.271	-13.271
$\|A_{fr}\| = 11$	3.808	3.622	3.622	-8.857	-13.315	-13.315

TABLE II. SYMMETRICAL INITIAL BATTERY SOCS ($B_{DSoC} = 0.1$)

β_{dSoC} = 0.1	Front Battery SoC_{end} [%]			Rear Battery SoC_{end} [%]		
	$\|A_{lr}\| = 1$	$\|A_{lr}\| = 3$	$\|A_{lr}\| = 11$	$\|A_{lr}\| = 1$	$\|A_{lr}\| = 3$	$\|A_{lr}\| = 11$
$\|A_{fr}\| = 1$	75.822	76.255	76.255	75.822	76.255	76.255
$\|A_{fr}\| = 3$	76.116	76.341	76.341	76.116	76.34	76.34
$\|A_{fr}\| = 11$	76.123	76.335	76.335	76.05	76.334	76.334
β_{dSoC} = 0.1	Average Battery dSoC [%]			dSoC Deviation [%]		
	$\|A_{lr}\| = 1$	$\|A_{lr}\| = 3$	$\|A_{lr}\| = 11$	$\|A_{lr}\| = 1$	$\|A_{lr}\| = 3$	$\|A_{lr}\| = 11$
$\|A_{fr}\| = 1$	4.178	3.745	3.745	0	-10.376	-10.376
$\|A_{fr}\| = 3$	3.884	3.66	3.66	-7.034	-12.409	-12.41
$\|A_{fr}\| = 11$	3.914	3.666	3.666	-6.328	-12.263	-12.263

TABLE III. SYMMETRICAL INITIAL BATTERY SOCS ($B_{DSoC} = 1.0$)

β_{dSoC} = 1.0	Front Battery SoC_{end} [%]			Rear Battery SoC_{end} [%]		
	$\|A_{lr}\| = 1$	$\|A_{lr}\| = 3$	$\|A_{lr}\| = 11$	$\|A_{lr}\| = 1$	$\|A_{lr}\| = 3$	$\|A_{lr}\| = 11$
$\|A_{fr}\| = 1$	75.822	76.255	76.255	75.822	76.255	76.255
$\|A_{fr}\| = 3$	75.838	76.255	76.256	75.838	76.255	76.256
$\|A_{fr}\| = 11$	75.836	76.255	76.256	75.836	76.255	76.256
β_{dSoC} = 1.0	Average Battery dSoC [%]			dSoC Deviation [%]		
	$\|A_{lr}\| = 1$	$\|A_{lr}\| = 3$	$\|A_{lr}\| = 11$	$\|A_{lr}\| = 1$	$\|A_{lr}\| = 3$	$\|A_{lr}\| = 11$
$\|A_{fr}\| = 1$	4.178	3.745	3.745	0	-10.376	-10.376
$\|A_{fr}\| = 3$	4.162	3.745	3.744	-0.384	-10.376	-10.381
$\|A_{fr}\| = 11$	4.164	3.745	3.744	-0.333	-10.376	-10.383

TABLE IV. ASYMMETRICAL INITIAL BATTERY SOCS ($B_{DSoC} = 0.1$)

β_{dSoC} = 0.1	Front Battery SoC_{end} [%]			Rear Battery SoC_{end} [%]		
	$\|A_{lr}\| = 1$	$\|A_{lr}\| = 3$	$\|A_{lr}\| = 11$	$\|A_{lr}\| = 1$	$\|A_{lr}\| = 3$	$\|A_{lr}\| = 11$
$\|A_{fr}\| = 1$	55.664	56.111	56.111	75.822	76.255	76.255
$\|A_{fr}\| = 3$	60.741	60.826	60.826	71.55	71.752	71.752
$\|A_{fr}\| = 11$	60.927	60.974	60.974	71.347	71.607	71.607
β_{dSoC} = 0.1	Average Battery dSoC [%]			dSoC Deviation [%]		
	$\|A_{lr}\| = 1$	$\|A_{lr}\| = 3$	$\|A_{lr}\| = 11$	$\|A_{lr}\| = 1$	$\|A_{lr}\| = 3$	$\|A_{lr}\| = 11$
$\|A_{fr}\| = 1$	4.257	3.817	3.817	0	-10.347	-10.347
$\|A_{fr}\| = 3$	3.855	3.711	3.711	-9.454	-12.818	-12.818
$\|A_{fr}\| = 11$	3.863	3.71	3.71	-9.259	-12.86	-12.86

TABLE V. DECREASED ENERGY EFFICIENCY OF FRONT LEFT MOTOR

β_{dSoC} = 0.1	Front Battery SoC_{end} [%]			Rear Battery SoC_{end} [%]		
	$\|A_{lr}\| = 1$	$\|A_{lr}\| = 3$	$\|A_{lr}\| = 11$	$\|A_{lr}\| = 1$	$\|A_{lr}\| = 3$	$\|A_{lr}\| = 11$
$\|A_{fr}\| = 1$	75.091	76.23	76.237	75.822	76.255	76.255
$\|A_{fr}\| = 3$	76.006	76.325	76.332	75.816	76.33	76.33
$\|A_{fr}\| = 11$	75.983	76.33	76.33	75.845	76.33	76.33
β_{dSoC} = 0.1	Average Battery dSoC [%]			dSoC Deviation [%]		
	$\|A_{lr}\| = 1$	$\|A_{lr}\| = 3$	$\|A_{lr}\| = 11$	$\|A_{lr}\| = 1$	$\|A_{lr}\| = 3$	$\|A_{lr}\| = 11$
$\|A_{fr}\| = 1$	4.544	3.757	3.754	0	-17.308	-17.383
$\|A_{fr}\| = 3$	4.089	3.672	3.669	-10.002	-19.175	-19.251
$\|A_{fr}\| = 11$	4.086	3.67	3.67	-10.069	-19.222	-19.222

A. Scenario 1: symmetrical initial battery state of charges

For simulation results in this scenario it is assumed that the initial state of charge for front and rear battery is equal to 80%. As shown in Section III.C, the scaling factor β_{dSoC} influences the symmetry of the batteries discharge. The simulation results for three different scaling factors ($\beta_{dSoC} \in \{0.0, 0.1, 1.0\}$) are summarized in Table I to III. As expected, by increasing the scaling factor β_{dSoC} the symmetry of battery discharge is increased, but the overall energy efficiency is decreased. A proper selection of the scaling factor β_{dSoC} for a given use case is dependent on the required batteries discharge symmetry and maximum tolerated delta state of charge.

For a powertrain topology with individually propelled axles it was shown in [8, 10] that the energy efficiency is maximized for the distribution factor $\alpha_{fr} = 0.0$ for low torque request and $\alpha_{fr} = 0.5$ for high torque requests. This torque distribution strategy corresponds to the simulation results with $|A_{lr}| = 1$ and $|A_{fr}| = 3$. As the simulation results show, the additional degree of freedom for torque distribution between left and right side electrical machines improves the efficiency in comparison to the torque distribution between front and rear axle only. Fig. 5 illustrates the comparison of the state of charge signals for the duration of the driving cycle. The blue line corresponds to the $|A_{fr}| = 1$ and $|A_{lr}| = 1$ torque distribution. The orange line corresponds to the torque distribution strategy proposed in this paper with $|A_{fr}| = 11$ and $|A_{lr}| = 11$ torque distribution and $\beta_{dSoC} = 0.1$.

B. Scenario 2: asymmetrical initial battery state of charges

The advantages of the proposed torque distribution control can be also seen when starting a driving cycle with asymmetrical initial battery state of charges. For the scenario 2 simulation results it is assumed that the start state of charge of front battery equals 60% and 80% for the rear battery. Fig. 6 illustrates the comparison of the state of charge signals for the duration of the driving cycle. The blue line corresponds to the $|A_{fr}| = 1$ and $|A_{lr}| = 1$ torque distribution. The orange line corresponds to the torque distribution strategy proposed in this paper with $|A_{fr}| = 11$ and $|A_{lr}| = 11$ torque distribution and $\beta_{dSoC} = 0.1$. Since the delta state of charge is high at the beginning of the driving cycle, the torque distribution strategy proposed in this paper tries to compensate the difference using the rear battery for the propulsion energy and recuperating more energy to the front battery. The end state of charge of the front battery is even higher than the initial state of charge while the energy efficiency is increased by approximately 13%. The simulation results for scenario 2 are summarized in Table IV.

C. Scenario 3: Decreased efficiency of front left motor

For simulation results in this scenario it is assumed that the efficiency of the front left electrical machine is decreased by 20%. The torque distribution control strategy as proposed in this paper reacts automatically to this fault by balancing the batteries discharge. Fig. 7 illustrates the comparison of the state of charge signals for the duration of the driving cycle. The blue

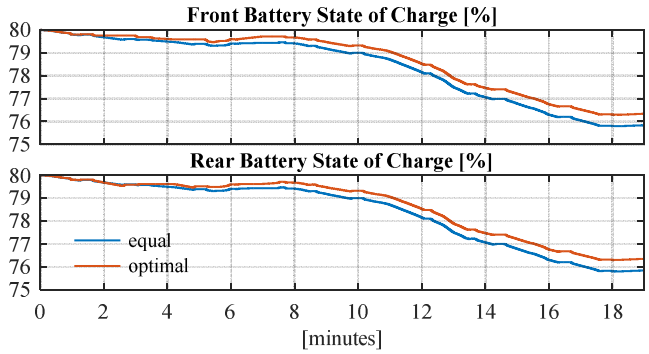

Fig. 5. Scenario 1: symmetrical initial state of charge of batteries.

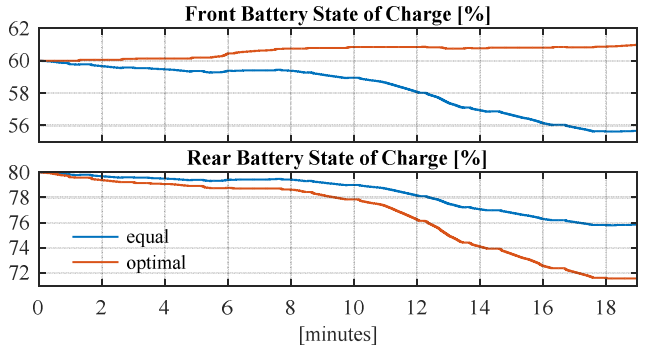

Fig. 6. Scenario 2: asymmetrical initial state of charge of batteries.

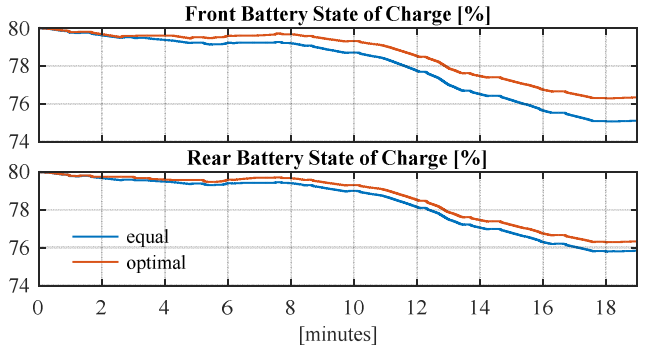

Fig. 7. Scenario 3: Decreased efficiency of front left electrical machine.

line corresponds to the $|A_{fr}| = 1$ and $|A_{lr}| = 1$ torque distribution. The orange line corresponds to the $|A_{fr}| = 11$ and $|A_{lr}| = 11$ torque distribution and $\beta_{dSoC} = 0.1$. By avoiding torque requests for the motor with decreased efficiency the battery discharge is balanced and the efficiency is increased by approximately 19%. The simulation results are summarized in Table V.

V. Conclusion

The work presented in this paper introduced a new optimal torque distribution strategy for the control of fail-operational powertrain topologies used for highly and fully automated driving. A mathematical model of the fail-operational powertrain was presented, which was then used for the definition of the optimization problem for torque distribution in normal and failure case operation. The goals of the optimization problem are to increase the driving efficiency and to ensure a symmetrical discharge of independent traction batteries. An online algorithm predicting the torque distribution profile for the entire driving cycle used for the safety based range extension was presented. The simulation results for different normal and failure case scenarios show a significant increase in the driving efficiency.

References

[1] Roland Berger GmbH, "A CEO agenda for the (r)evolution of the automotive ecosystem," Munich, Germany, 2016.

[2] Taxonomy and Definitions for Terms Related to Driving Automation Systems for On-Road Motor Vehicles, SAE International Standard J3016 SEP2016, 2016.

[3] Road vehicles - Functional safety - Part 3: Concept phase, ISO International Standard 26262-3, 2011.

[4] A. Kilic, T. Shen and K. Gorelik, "Entwicklung eines fail-operational Bordnetzes für autonomes Fahren," in *8. VDI/VDE Fachtungung "AUTOREG 2017 - Automatisiertes Fahren und vernetzte Mobilität"*, Berlin, Germany, 2017.

[5] K. Gorelik, A. Kilic and R. Obermaisser, "Energy Management System for Automated Driving - Optimal and Adaptive Control Strategy for Normal and Failure Case Operation," in *11th Annual IEEE International Systems Conference*, Montreal, Canada, 2017, pp. 597-604.

[6] K. Gorelik, A. Kilic and R. Obermaisser, "Modeling and Simulation of Optimal and Adaptive Real-Time Energy Management System for Automated Driving," in *IEEE Transportation Electrification Conference and Expo*, Chicago, USA, 2017, pp. 356-363.

[7] K. Gorelik, A. Kilic and R. Obermaisser, "Dynamic and Route Based Range Prediction for Automated Electric Vehicles - Connected Energy Management System with Range Extension for Improved Safety," in *Vehicle Power and Propulsion Conference*, Belfort, France, 2017.

[8] X. Yuan and J. Wang, "Torque Distribution Strategy for a Front- and Rear-Wheel-Driven Electric Vehicle," *IEEE Transactions on Vehicular Technology,* vol. 61, no. 8, pp. 3365-3374, October 2012.

[9] S. Koehler, A. Viehl, O. Bringmann and W. Rosenstiel, "Optimized Recuperation Strategy for (Hybrid) Electric Vehicles Based on Intelligent Sensors," in *12th International Conference on Control, Automation and Systems*, Jeju Island, Korea, 2012.

[10] S. Koehler, A. Viehl, O. Bringmann and W. Rosenstiel, "Energy-Efficient Torque Distribution for Axle-Individually Propelled Electric Vehicles," in *Intelligent Vehicles Symposium*, Dearborn, USA, 2014.

[11] L. Guo, X. Lin, P. Ge, Y. Qiao, L. Xu and J. Li, "Torque Distribution for Electric Vehicle with Four In-Wheel Motors by Considering Energy Optimization and Dynamics Performance," in *IEEE Intelligent Vehicles Symposium*, Redondo Beach, USA, 2017, pp. 1619-1624.

[12] Y.-P. Yang, Y.-C. Shih and J.-M. Chen, "Real-time torque-distribution strategy for a pure electric vehicle with multiple traction motors by particle swarm optimisation," *IET Electrical Systems in Transportation,* vol. 6, no. 2, pp. 76-87, 2016.

[13] J. Ludwig, "Elektronischer Horizont für vorausschauende Kartendaten," *ATZelektronik,* vol. 9, no. 7, pp. 24-27, 2014.

[14] C. Ress, D. Balzer, A. Bracht, S. Durekovic and J. Löwenau, "ADASIS Protocol for Advanced In-Vehicle Applications," in *15th World Congress on Intelligent Transport Systems*, New York, USA, 2008.

[15] C. Ress, A. Etemad, D. Kuck and J. Requero, "Electronic Horizon - Providing Digital Map Data for ADAS Applications," in *2nd International Workshop on Intelligent Vehicle Control Systems*, Madeira, Portugal, 2008.

[16] L. Guzzella and A. Sciarretta, Vehicle Propulsion System - Introduction to Modeling and Optimization, 3rd ed., Berlin – Heidelberg, Springer, 2013.